

Trans-Pacific transport of Asian dust and CO: Accumulation of biomass burning CO in subtropics and dipole structure of transport

J. Nam¹, Y. Wang¹, C. Luo¹, and D.A. Chu²

¹School of Earth and Atmospheric Sciences, Georgia Institute of Technology, Atlanta, GA, 30332, USA

²NASA Goddard Space Flight Center, Greenbelt, MD, 20771, USA

In Figure S1, we show the biomass burning emissions from the GFED inventories over East Asia for April 2003. In Figure S2, we show the monthly mean CO columns of tagged CO tracers over the Pacific for May 2003. In Figure S3, we show the distribution of CO transport over the Pacific in the sensitivity simulation of doubling anthropogenic CO emissions from SE China. In Figure S4, we compare GEOS-4 wind vectors at 500 hPa and 900 hPa used in model simulations and the corresponding wind vectors with the NCEP reanalysis during 1-2 May 2003. In Figure S5, we show the forward trajectories of dust released from the Gobi and Taklimakan deserts calculated using the HYSPLIT model. In Figure S6, we compare CO mixing ratio from model simulation to ESRL observations. In Figure S7, we compare aerosol extinction from model simulation to observation in ESRL sites and MODIS. In Figure S8, we compare model AOD to AERONET and MODIS AOD in four AERONET sites.

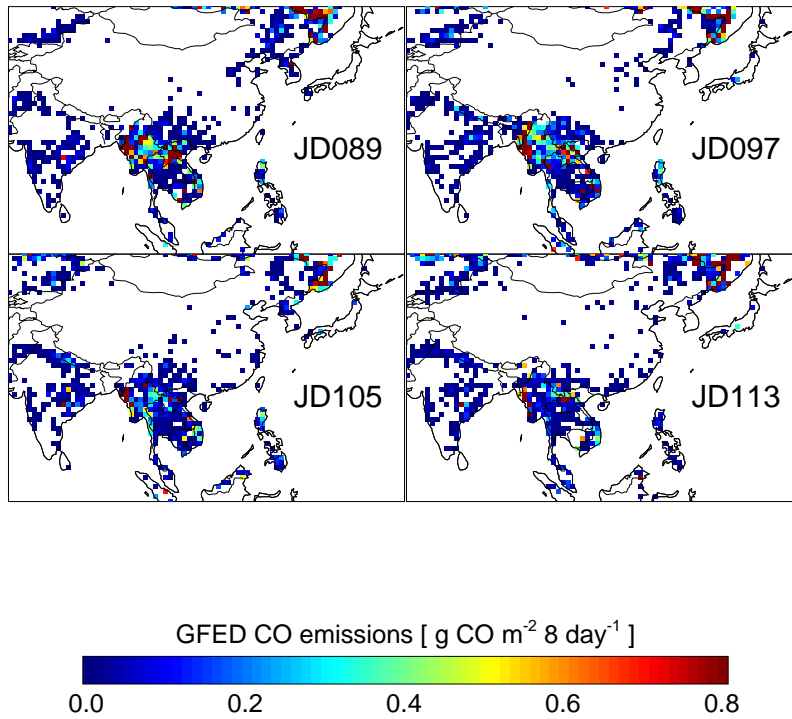


Fig. 1. Biomass burning CO emissions from the GFED inventories over East Asia. Values are reported as 8-day averages of 30 March-6 April (JD089), 7-14 April (JD097), 15-22 April (JD105), and 23-30 April 2003 (JD113). The original GFED inventory, without enhanced emissions in Burma, is shown here.

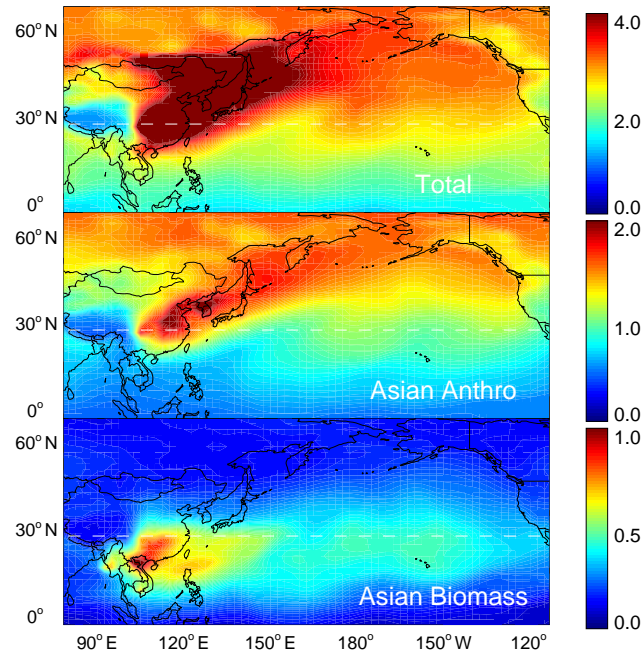


Fig. 2. Monthly mean total CO columns [10^{18} molecules cm^{-2}] over the Pacific for May 2003 (first) and the corresponding CO columns from anthropogenic sources in Asia (second) and from biomass burning sources in southeast Asia (third) in the tagged CO simulation. The biomass burning emissions in southeast Asia from the GFED inventory was increased by a factor of 8 in April.

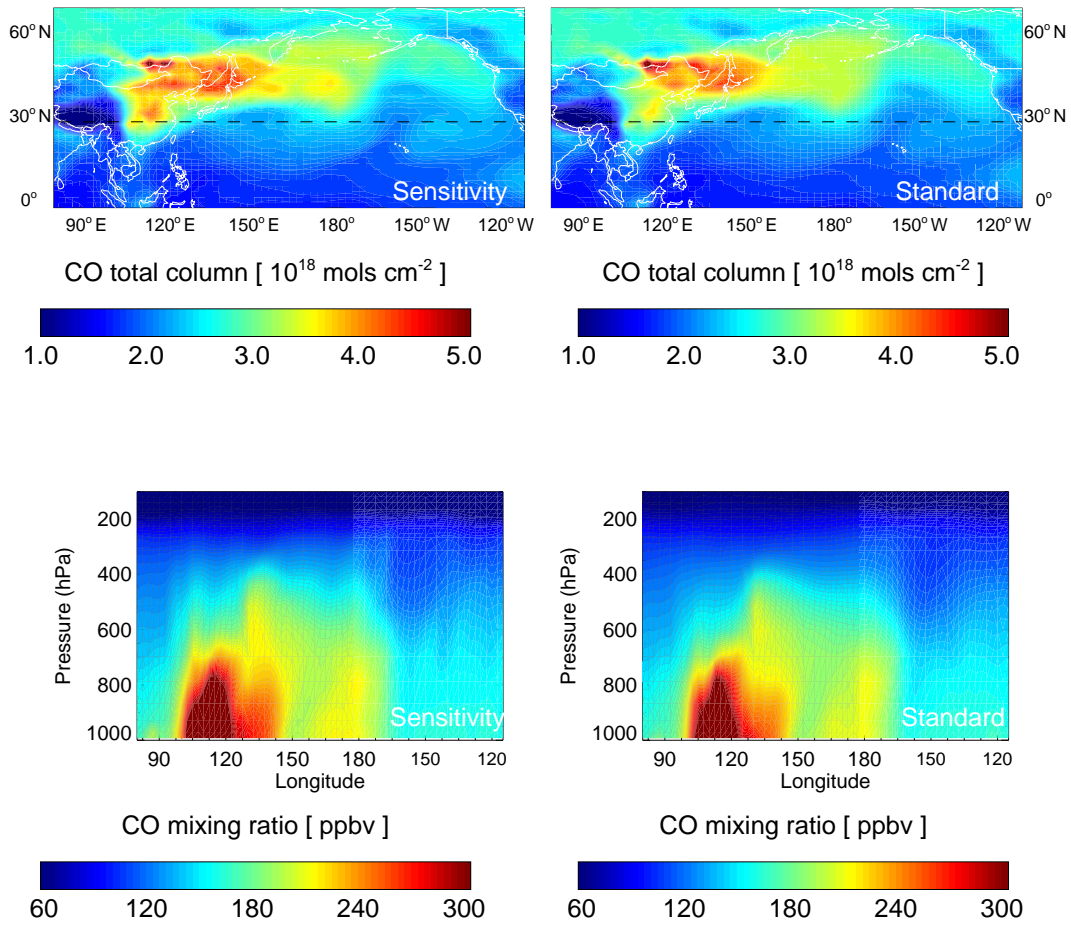


Fig. 3. Horizontal (first row) and vertical (second row) distributions of CO transport in the sensitivity (first column) and standard simulations (second column). In the sensitivity simulation, the anthropogenic emissions of CO from SE China are doubled in the previous 6 months.

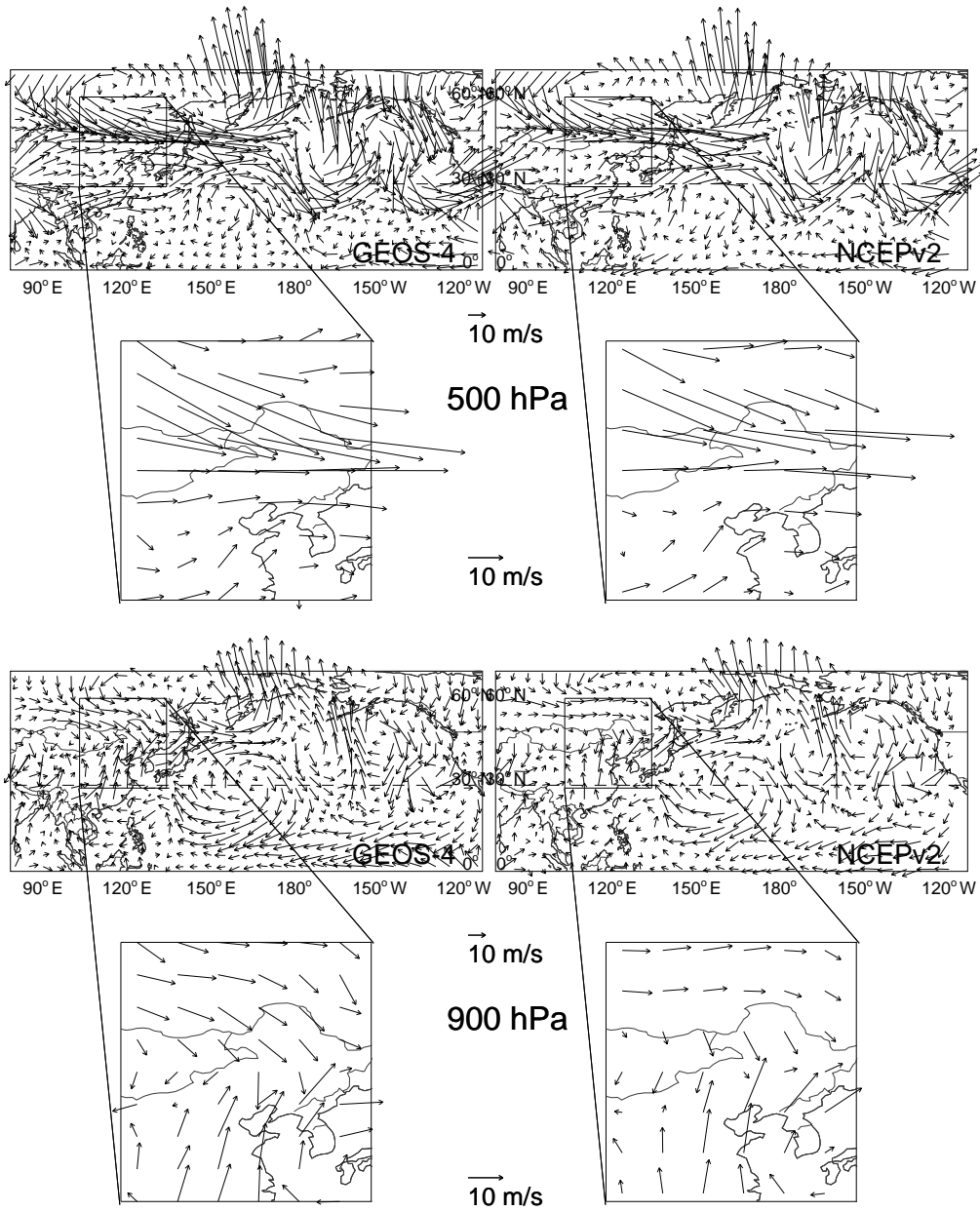


Fig. 4. GEOS-4 wind vectors (left) at 500 hPa (above) and 900 hPa (below) used in model simulations and the corresponding wind vectors from the NCEP reanalysis (right) during 1-2 May 2003.

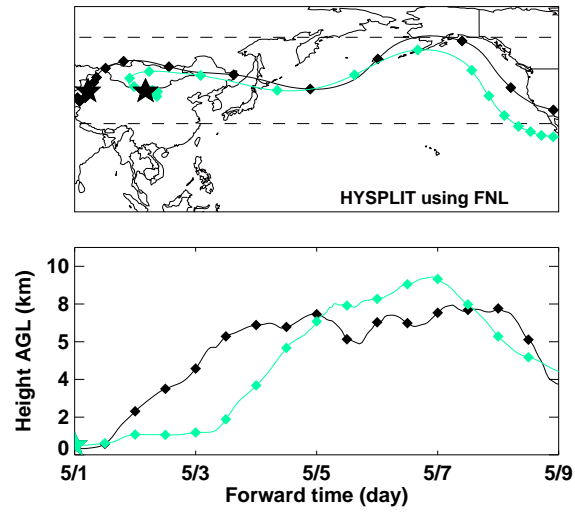


Fig. 5. Forward trajectory of dust release at Gobi (Green) and Taklimakan (Black) deserts from May 1 to May 8, 2003 using HYSPLIT model with FNL meteorological dataset.

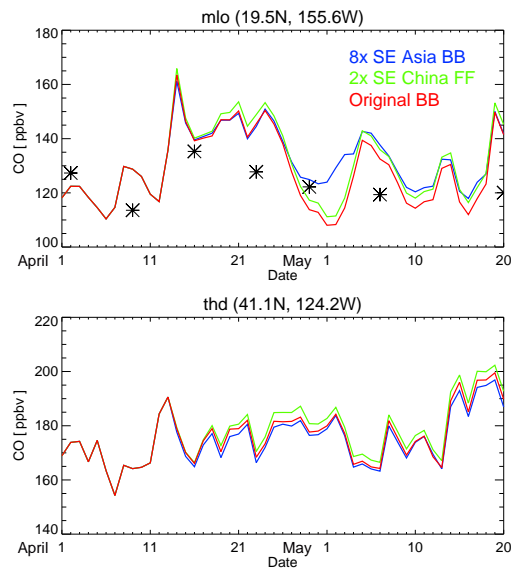


Fig. 6. Comparison of CO mixing ratio simulated with GEOS-Chem (lines) using three different schemes of CO emissions with ESRL surface measurements (asterisks) from 1 April to 20 May 2003. Description of different simulations are provided in Figure 3.

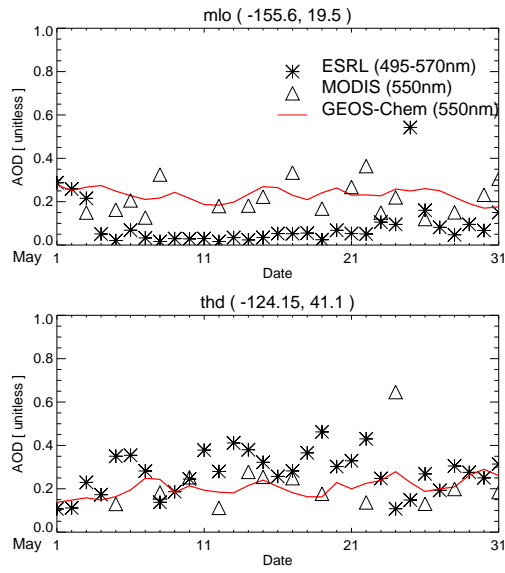


Fig. 7. Comparison of aerosol extinction simulated with GEOS-Chem (lines) with observation from ESRL surface sites (asterisks) and MODIS (triangles) for May 2003.

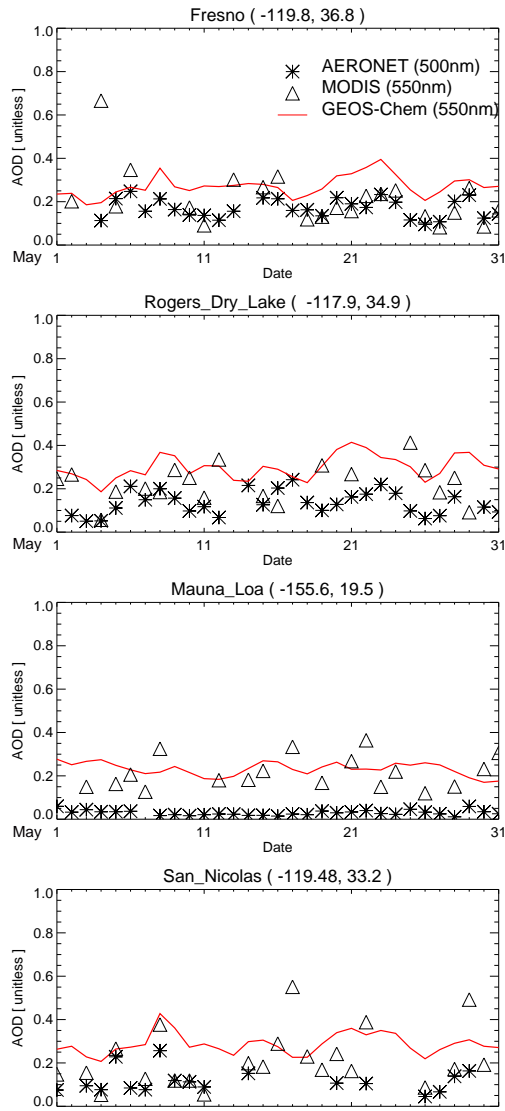


Fig. 8. Comparison of simulated AOD (lines) with observed AOD in AERONET (asterisks) and MODIS (triangles) for May 2003.